Journal of Sound and Vibration (2000) **229**(1), 3–19
Article No. jsvi.1999.2328, available online at http://www.idealibrary.com on IDEAL®

ACOUSTIC ATTENUATION PERFORMANCE OF CIRCULAR EXPANSION CHAMBERS WITH SINGLE-INLET AND DOUBLE-OUTLET

A. SELAMET AND Z. L. JI

Department of Mechanical Engineering and The Center for Automotive Research, The Ohio State University, Columbus, OH 43210-1107, *U.S.A.*

(*Received* 21 *May* 1998, *and in final form* 12 *April* 1999)

Expansion chambers with single-inlet and double-outlet provide desirable broadband acoustic attenuation similar to simple (single inlet/outlet) chambers and reduce the flow noise and back pressure in exhaust systems. The present study develops a three-dimensional analytical approach to determine the transmission loss of circular expansion chambers with single-inlet and double-outlet, which couples the continuity conditions of the acoustic pressure and particle velocity at the inlet and outlets with the orthogonality relations of Fourier–Bessel functions. The analytical results are compared with the boundary element predictions. The acoustic attenuation of the expansion chambers with single-inlet and double-outlet is then investigated in detail as a function of the chamber length and the locations of inlet and outlets.

1. INTRODUCTION

The expansion chambers have been extensively used as silencers in the exhaust systems of internal combustion engines. A number of analytical and experimental studies have investigated the effect of geometry on the acoustic attenuation performance of conventional expansion chambers (with single inlet/outlet) (see, for example, reference [1–5]). The studies on the circular configurations demonstrated that the long expansion chambers exhibit repeating attenuation domes dictated by reflections in the axial direction below the cut-off frequency of the first higher order mode, while the short expansion chambers show the dominant wave propagation along the transverse direction. Numerical techniques, such as the finite element method (FEM) [6, 7] and the boundary element method (BEM) [8–10], have also been successfully used to predict the acoustic attenuation performance of expansion chambers. For the expansion chambers with single inlet/outlet, the boundary element predictions of transmission loss show a good agreement with the analytical and experimental results [1, 3].

For a given chamber size, reducing the duct diameters would increase the acoustic attenuation of airborne sound as a result of increases in the wave

0022-460X/00/010003 + 17 $35.00/0

reflections. This would, however, compete with the need to control the aerodynamic noise and to keep the back pressure at reasonably low levels. The flow noise (power), for example, due to spoilers inside the ducts has been shown to be proportional to $U^3 f(\mathrm{Ma})$ [11], where U is the average velocity in the duct and Ma is the Mach number. For plane wave propagation below the first cut-off frequency, $f(\mathrm{Ma}) = \mathrm{Ma}$, whereas $f(\mathrm{Ma}) = \mathrm{Ma}^3$ above this frequency. Measurements of flow noise in engine exhaust systems [12, 13] have yielded typically $f(\mathrm{Ma}) = \mathrm{Ma}^{1\cdot5}$, in agreement with the range defined by Nelson and Morfey [11] at relatively low Mach numbers ($\leqslant 0{\cdot}3$). The source of flow losses in the silencers, such as expansion chambers, is predominantly the flow separation from walls. Pressure drop for this mechanism is usually proportional to U^2. The energy losses due to different elements then add up to generate the back pressure engine cylinder experiences in the exhaust ports. The higher backpressure increases the pumping work, thus reduces the engine performance. Both flow noise and back pressure are then strongly dependent on the velocity, typically playing a significant role from mid-speed range on. The increase in the exit cross-sectional area with double-outlet expansion chambers reduces the velocity, and therefore is expected to improve on the flow noise and backpressure.

It appears, however, that the acoustic attenuation performance of the foregoing chambers with double-outlet has not been investigated in detail. The objective of the present study is to develop a *three-dimensional analytical approach* to determine the transmission loss of *the circular expansion chambers with single-inlet and double-outlet* in the absence of mean flow, and then use this approach to investigate the effect of the chamber length and the locations of inlet and outlets on the acoustic attenuation performance of expansion chambers. The present work also employs the BEM to examine the analytical approach.

Following the Introduction, section 2 describes the analytical approach, section 3 compares transmission loss results from the analytical approach with the boundary element predictions and discusses the effects of the chamber length and the locations of inlet and outlets on the acoustic attenuation performance of the circular expansion chambers with single-inlet and double-outlet. The study is concluded in section 4 with some final remarks.

2. ANALYTICAL APPROACH

The analytical solution to the Helmholtz equation for three-dimensional sound propagation in a cylindrical duct is described in Appendix A. For a circular expansion chamber with single-inlet and double-outlet ducts shown in Figure 1, equations (A2), (A3), (A5) and (A6) can then be used for acoustic pressures and particle velocities in the inlet duct, expansion chamber and outlet ducts.

At the expansion, the pressure and velocity continuity conditions reveal

$$(P_A + P_B)|_{z_1=0} = (P_C + P_D)|_{z_1=0} \quad (\text{on } S_1), \tag{1}$$

$$(U_A + U_B)|_{z_1=0} = (U_C + U_D)|_{z_1=0} \quad (\text{on } S_1), \tag{2}$$

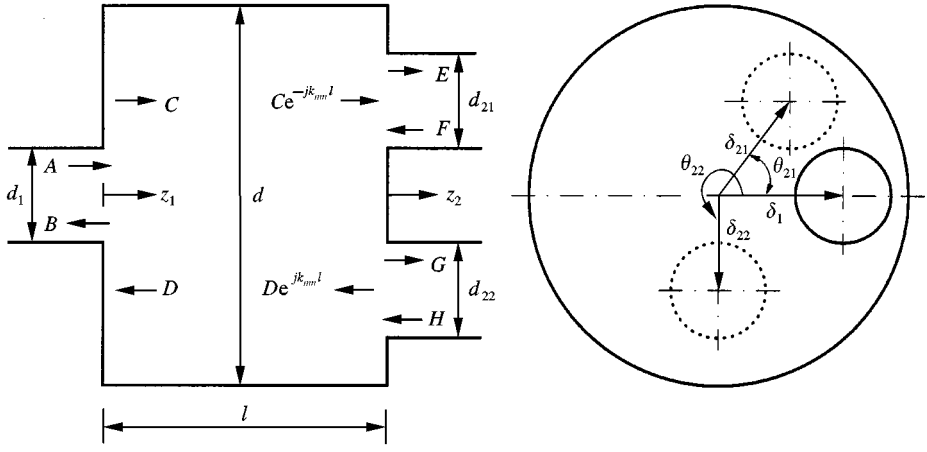

Figure 1. Circular expansion chamber with single-inlet and double-outlet.

and the velocity boundary condition requires

$$(U_C + U_D)|_{z_1=0} = 0 \quad (\text{on } S - S_1). \tag{3}$$

Similar to the simple expansion chamber [2], multiply both sides of equation (1) by $J_t(\alpha_{ts}r_1/a_1)e^{-jt\varphi}$ and integrate over S_1 to get, for $t = 0, 1, \ldots, \infty$ and $s = 0, 1, \ldots, \infty$,

$$[A_{ts}^+ + B_{ts}^+](a_1^2/2)(1 - t^2/\alpha_{ts}^2)J_t(\alpha_{ts}) = \sum_{m=0}^{\infty}\sum_{n=0}^{\infty}(C_{mn}^+ + D_{mn}^+)J_{m+t}(\alpha_{mn}\delta_1/a)\mathfrak{R}_1$$
$$+ \sum_{m=1}^{\infty}\sum_{n=0}^{\infty}(C_{mn}^- + D_{mn}^-)(-1)^t J_{m-t}(\alpha_{mn}\delta_1/a)\mathfrak{R}_1, \tag{4}$$

multiplying both sides of equation (1) by $J_t(\alpha_{ts}r_1/a_1)e^{jt\varphi}$ and integrating over S_1, the following equation can be obtained, for $t = 1, 2, \ldots, \infty$ and $s = 0, 1, \ldots, \infty$:

$$[A_{ts}^- + B_{ts}^-](a_1^2/2)(1 - t^2/\alpha_{ts}^2)J_t(\alpha_{ts}) = \sum_{m=0}^{\infty}\sum_{n=0}^{\infty}(C_{mn}^+ + D_{mm}^+)(-1)^t J_{m-t}(\alpha_{mn}\delta_1/a)\mathfrak{R}_1$$
$$+ \sum_{m=1}^{\infty}\sum_{n=0}^{\infty}(C_{mn}^- + D_{mn}^-)J_{m+t}(\alpha_{mn}\delta_1/a)\mathfrak{R}_1, \tag{5}$$

where

$$\mathfrak{R}_1 = \begin{cases}(\alpha_{mn}a_1/a)J_t'(\alpha_{mn}a_1/a)/[(\alpha_{ts}/a_1)^2 - (\alpha_{mn}/a)^2] & \text{for } \alpha_{mn}/a \neq \alpha_{ts}/a_1,\\ (a_1^2/2)(1 - t^2/\alpha_{ts}^2)J_t(\alpha_{ts}) & \text{for } \alpha_{mn}/a = \alpha_{ts}/a_1.\end{cases}$$

For the velocity conditions, multiply both equations (2) and (3) by $J_t(\alpha_{ts}r/a)e^{-jt\theta}$ and integrate them over S_1 and $S-S_1$, respectively, and then add these two integral equations to yield, for $t=0, 1, \ldots, \infty$ and $s=0, 1, \ldots, \infty$,

$$\sum_{m=0}^{\infty}\sum_{n=0}^{\infty} k_{1,mn}(A_{mn}^{+}-B_{mn}^{+})J_{m+t}(\alpha_{ts}\delta_1/a)\mathfrak{R}_2 + \sum_{m=1}^{\infty}\sum_{n=0}^{\infty} k_{1,mn}(A_{mn}^{-}-B_{mn}^{-})(-1)^t J_{m-t}(\alpha_{ts}\delta_1/a)\mathfrak{R}_2 = k_{ts}[C_{ts}^{+}-D_{ts}^{+}](a^2/2)(1-t^2/\alpha_{ts}^2)J_t^2(\alpha_{ts}), \tag{6}$$

multiply both equations (2) and (3) by $J_t(\alpha_{ts}r/a)e^{jt\theta}$ and integrate them over S_1 and $S-S_1$, respectively, and then add them to get, for $t=1, 2, \ldots, \infty$ and $s=0, 1, \ldots, \infty$,

$$\sum_{m=0}^{\infty}\sum_{n=0}^{\infty} k_{1,mn}(A_{mn}^{+}-B_{mn}^{+})(-1)^t J_{m-t}(\alpha_{ts}\delta_1/a)\mathfrak{R}_2 + \sum_{m=1}^{\infty}\sum_{n=0}^{\infty} k_{1,mm}(A_{mn}^{-}-B_{mn}^{-})J_{m+t}(\alpha_{ts}\delta_1/a)\mathfrak{R}_2 = k_{ts}[C_{ts}^{-}-D_{ts}^{-}](a^2/2)(1-t^2/\alpha_{ts}^2)J_t^2(\alpha_{ts}), \tag{7}$$

where

$$\mathfrak{R}_2 = \begin{cases} (\alpha_{ts}a_1/a)J_m(\alpha_{mn})J_m'(\alpha_{ts}a_1/a)/[(\alpha_{mn}/a_1)^2-(\alpha_{ts}/a)^2] & \text{for } \alpha_{mn}/a_1 \neq \alpha_{ts}/a, \\ (a_1^2/2)(1-m^2/\alpha_{mn}^2)J_m^2(\alpha_{mn}) & \text{for } \alpha_{mn}/a_1 = \alpha_{ts}/a_1, \end{cases}$$

and $k_{1,mn}=k[1-(\alpha_{mn}/ka_1)^2]^{1/2}$ is the axial wavenumber in the inlet duct.

At the contraction, the pressure and velocity continuity conditions reveal

$$(P_C+P_D)|_{z_1=l} = (P_E+P_F)|_{z_2=0} \quad (\text{on } S_{21}), \tag{8}$$

$$(P_C+P_D)|_{z_1=l} = (P_G+P_H)|_{z_2=0} \quad (\text{on } S_{22}), \tag{9}$$

$$(U_C+U_D)|_{z_1=l} = (U_E+U_F)|_{z_2=0} \quad (\text{on } S_{21}), \tag{10}$$

$$(U_C+U_D)|_{z_1=l} = (U_G+U_H)|_{z_2=0} \quad (\text{on } S_{22}), \tag{11}$$

and the velocity boundary condition requires

$$(U_C+U_D)|_{z_1=l} = 0 \quad (\text{on } S-S_{21}-S_{22}). \tag{12}$$

For the pressure conditions at outlets, using the same procedure as the inlet, equation (8) gives, for $t = 0, 1, \ldots, \infty$ and $s = 0, 1, \ldots, \infty$,

$$\sum_{m=0}^{\infty}\sum_{n=0}^{\infty}(C_{mn}^{+}\mathrm{e}^{-\mathrm{j}k_{mn}l} + D_{mn}^{+}\mathrm{e}^{\mathrm{j}k_{mn}l})J_{m+t}(\alpha_{mn}\delta_{21}/a)\mathrm{e}^{-\mathrm{j}m\theta_{21}}\mathfrak{R}_3 + \sum_{m=1}^{\infty}\sum_{n=0}^{\infty}(C_{mn}^{-}\mathrm{e}^{-\mathrm{j}k_{mn}l} + D_{mn}^{-}\mathrm{e}^{\mathrm{j}k_{mn}l})(-1)^t J_{m-t}(\alpha_{mn}\delta_{21}/a)\mathrm{e}^{\mathrm{j}m\theta_{21}}\mathfrak{R}_3 = (E_{ts}^{+} + F_{ts}^{+})(a_{21}^2/2)(1 - t^2/\alpha_{ts}^2)J_t(\alpha_{ts}), \tag{13}$$

and for $t = 1, 2, \ldots, \infty$ and $s = 0, 1, \ldots, \infty$,

$$\sum_{m=0}^{\infty}\sum_{n=0}^{\infty}(C_{mn}^{+}\mathrm{e}^{-\mathrm{j}k_{mn}l} + D_{mn}^{+}\mathrm{e}^{\mathrm{j}k_{mn}l})(-1)^t J_{m-t}(\alpha_{mn}\delta_{21}/a)\mathrm{e}^{-\mathrm{j}m\theta_{21}}\mathfrak{R}_3 + \sum_{m=1}^{\infty}\sum_{n=0}^{\infty}(C_{mn}^{-}\mathrm{e}^{-\mathrm{j}k_{mn}l} + D_{mn}^{-}\mathrm{e}^{\mathrm{j}k_{mn}l})J_{m+t}(\alpha_{mn}\delta_{21}/a)\mathrm{e}^{\mathrm{j}m\theta_{21}}\mathfrak{R}_3 = (E_{ts}^{-} + F_{ts}^{-})(a_{21}^2/2)(1 - t^2/\alpha_{ts}^2)J_t(\alpha_{ts}), \tag{14}$$

where

$$\mathfrak{R}_3 = \begin{cases}(\alpha_{mn}a_{21}/a)J_t'(\alpha_{mn}a_{21}/a)/[(\alpha_{ts}/a_{21})^2 - (\alpha_{mn}/a)^2] & \text{for } \alpha_{mn}/a \neq \alpha_{ts}/a_{21},\\ (a_{21}^2/2)(1 - t^2/\alpha_{ts}^2)J_t(\alpha_{ts}) & \text{for } \alpha_{mn}/a = \alpha_{ts}/a_{21}.\end{cases}$$

Similarly, equation (9) gives, for $t = 0, 1, \ldots, \infty$ and $s = 0, 1, \ldots, \infty$,

$$\sum_{m=0}^{\infty}\sum_{n=0}^{\infty}(C_{mn}^{+}\mathrm{e}^{-\mathrm{j}k_{mn}l} + D_{mn}^{+}\mathrm{e}^{\mathrm{j}k_{mn}l})J_{m+t}(\alpha_{mn}\delta_{22}/a)\mathrm{e}^{-\mathrm{j}m\theta_{22}}\mathfrak{R}_4 + \sum_{m=1}^{\infty}\sum_{n=0}^{\infty}(C_{mn}^{-}\mathrm{e}^{-\mathrm{j}k_{mn}l} + D_{mn}^{-}\mathrm{e}^{\mathrm{j}k_{mn}l})(-1)^t J_{m-t}(\alpha_{mn}\delta_{22}/a)\mathrm{e}^{\mathrm{j}m\theta_{22}}\mathfrak{R}_4 = (G_{ts}^{+} + H_{ts}^{+})(a_{22}^2/2)(1 - t^2/\alpha_{ts}^2)J_t(\alpha_{ts}), \tag{15}$$

and for $t = 1, 2, \ldots, \infty$ and $s = 0, 1, \ldots, \infty$,

$$\sum_{m=0}^{\infty}\sum_{n=0}^{\infty}(C_{mn}^{+}\mathrm{e}^{-\mathrm{j}k_{mn}l} + D_{mn}^{+}\mathrm{e}^{\mathrm{j}k_{mn}l})(-1)^t J_{m-t}(\alpha_{mn}\delta_{22}/a)\mathrm{e}^{-\mathrm{j}m\theta_{22}}\mathfrak{R}_4 + \sum_{m=1}^{\infty}\sum_{n=0}^{\infty}(C_{mn}^{-}\mathrm{e}^{-\mathrm{j}k_{mn}l} + D_{mn}^{-}\mathrm{e}^{\mathrm{j}k_{mn}l})J_{m+t}(\alpha_{mn}\delta_{22}/a)\mathrm{e}^{\mathrm{j}m\theta_{22}}\mathfrak{R}_4 = (G_{ts}^{-} + H_{ts}^{-})(a_{22}^2/2)(1 - t^2/\alpha_{ts}^2)J_t(\alpha_{ts}), \tag{16}$$

where

$$\mathfrak{R}_4 = \begin{cases} (\alpha_{mn}a_{22}/a)J_t'(\alpha_{mn}a_{22}/a)/[(\alpha_{ts}/a_{22})^2 - (\alpha_{mn}/a)^2] & \text{for } \alpha_{mn}/a \neq \alpha_{ts}/a_{22}, \\ (a_{22}^2/2)(1 - t^2/\alpha_{ts}^2)J_t(\alpha_{ts}) & \text{for } \alpha_{mn}/a = \alpha_{ts}/a_{22}. \end{cases}$$

For the velocity conditions, multiply equations (10), (11) and (12) by $J_t(\alpha_{ts}r/a)\mathrm{e}^{-\mathrm{j}t\theta}\,\mathrm{d}S$, and integrate them over S_{21}, S_{22} and $S - S_{21} - S_{22}$, respectively, and then add these three integral equations to give, for $t = 0, 1, \ldots, \infty$ and $s = 0, 1, \ldots, \infty$,

$$\begin{aligned} & k_{ts}[C_{ts}^+\mathrm{e}^{-\mathrm{j}k_{ts}l} - D_{ts}^+\mathrm{e}^{\mathrm{j}k_{ts}l}](a^2/2)(1 - t^2/\alpha_{ts}^2)J_t^2(\alpha_{ts}) \\ & \quad = \sum_{m=0}^{\infty}\sum_{n=0}^{\infty} k_{21,mn}(E_{mn}^+ - F_{mn}^+)J_{m+t}(\alpha_{ts}\delta_{21}/a)\mathfrak{R}_5\mathrm{e}^{\mathrm{j}t\theta_{21}} \\ & \qquad + \sum_{m=1}^{\infty}\sum_{n=0}^{\infty} k_{21,mn}(E_{mn}^- - F_{mn}^-)(-1)^t J_{m-t}(\alpha_{ts}\delta_{21}/a)\mathfrak{R}_5\mathrm{e}^{\mathrm{j}t\theta_{21}} \\ & \qquad + \sum_{m=0}^{\infty}\sum_{n=0}^{\infty} k_{22,mn}(G_{mn}^+ - H_{mn}^+)J_{m+t}(\alpha_{ts}\delta_{22}/a)\mathfrak{R}_6\mathrm{e}^{\mathrm{j}t\theta_{22}} \\ & \qquad + \sum_{m=1}^{\infty}\sum_{n=0}^{\infty} k_{22,mn}(G_{mn}^- - H_{mn}^-)(-1)^t J_{m-t}(\alpha_{ts}\delta_{22}/a)\mathfrak{R}_6\mathrm{e}^{\mathrm{j}t\theta_{22}}. \end{aligned} \tag{17}$$

Similarly, multiply equations (10), (11) and (12) by $J_t(\alpha_{ts}r/a)\mathrm{e}^{\mathrm{j}t\theta}\,\mathrm{d}S$, and integrate them over S_{21}, S_{22} and $S - S_{21} - S_{22}$, respectively, and then add them to get, for $t = 1, 2, \ldots, \infty$ and $s = 0, 1, \ldots, \infty$,

$$\begin{aligned} & k_{ts}[C_{ts}^-\mathrm{e}^{-\mathrm{j}k_{ts}l} - D_{ts}^-\mathrm{e}^{\mathrm{j}k_{ts}l}](a^2/2)(1 - t^2/\alpha_{ts}^2)J_t^2(\alpha_{ts}) \\ & \quad = \sum_{m=0}^{\infty}\sum_{n=0}^{\infty} k_{21,mn}(E_{mn}^+ - F_{mn}^+)(-1)^t J_{m-t}(\alpha_{ts}\delta_{21}/a)\mathfrak{R}_5\mathrm{e}^{\mathrm{j}t\theta_{21}} \\ & \qquad + \sum_{m=1}^{\infty}\sum_{n=0}^{\infty} k_{21,mn}(E_{mn}^- - F_{mn}^-)J_{m+t}(\alpha_{ts}\delta_{21}/a)\mathfrak{R}_5\mathrm{e}^{\mathrm{j}t\theta_{21}} \\ & \qquad + \sum_{m=0}^{\infty}\sum_{n=0}^{\infty} k_{22,mn}(G_{mn}^+ - H_{mn}^+)(-1)^t J_{m-t}(\alpha_{ts}\delta_{22}/a)\mathfrak{R}_6\mathrm{e}^{\mathrm{j}t\theta_{22}} \\ & \qquad + \sum_{m=1}^{\infty}\sum_{n=0}^{\infty} k_{22,mn}(G_{mn}^- - H_{mn}^-)J_{m+t}(\alpha_{ts}\delta_{22}/a)\mathfrak{R}_6\mathrm{e}^{\mathrm{j}t\theta_{22}}. \end{aligned} \tag{18}$$

In equations (17) and (18),

$$\mathfrak{R}_5 = \begin{cases} (\alpha_{ts}a_{21}/a)J_m(\alpha_{mn})J_m'(\alpha_{ts}a_{21}/a)/[(\alpha_{mn}/a_{21})^2 - (\alpha_{ts}/a)^2] & \text{for } \alpha_{mn}/a_{21} \neq \alpha_{ts}/a, \\ (a_{21}^2/2)(1 - m^2/\alpha_{mn}^2)J_m^2(\alpha_{mn}) & \text{for } \alpha_{mn}/a_{21} = \alpha_{ts}/a, \end{cases}$$

$$\mathfrak{R}_6 = \begin{cases} (\alpha_{ts}a_{22}/a)J_m(\alpha_{mn})J_m'(\alpha_{ts}a_{22}/a)/[(\alpha_{mn}/a_{22})^2 - (\alpha_{ts}/a)^2] & \text{for } \alpha_{mn}/a_{22} \neq \alpha_{ts}/a, \\ (a_{22}^2/2)(1 - m^2/\alpha_{mn}^2)J_m^2(\alpha_{mn}) & \text{for } \alpha_{mn}/a_{22} = \alpha_{ts}/a, \end{cases}$$

and $k_{21,mn} = k[1 - (\alpha_{mn}/ka_{21})^2]^{1/2}$, $k_{22,mn} = k[1 - (\alpha_{mn}/ka_{22})^2]^{1/2}$ are the axial wavenumbers in outlet ducts.

To determine the transmission loss of the expansion chamber with double-outlet: (1) the dimensions of the inlet duct are assumed such that the incoming wave A is planar, and its magnitude A_{00}^{+} is chosen to be unity for convenience, and (2) the anechoic terminations are imposed at the two exits of the chamber by setting the reflected waves F and H to zero. Thus, equations (4)–(7) and (13)–(18) give a large (theoretically infinite) number of relations $5(2t + 1)(s + 1)$ for a large number of unknowns $5(2m + 1)(n + 1)$. The unknowns are the pressure magnitudes for incident and reflected waves in the inlet duct, chamber, and outlet ducts (B_{mn}, C_{mn}, D_{mn}, E_{mn} and G_{mn}). Since the higher modes have a diminishing effect on the solution, t and m can be truncated to p terms and s and n to q terms, resulting in $5(2p + 1)(q + 1)$ equations with $5(2p + 1)(q + 1)$ unknowns. The number of terms, p and q, needed for a converged solution depend both on the magnitude of the area transition and the length of the chamber. For the geometries and frequencies investigated here, $p = 5$ and $q = 5$ were found to be sufficient. Once equations (4)–(7) and (13)–(18) are solved, the transmission loss is determined in the centers of ducts by

$$TL = -10\log_{10}\left\{(a_{21}/a_1)^2\left|\sum_{n=0}^{p} E_{0n}^{+}\mathrm{e}^{-\mathrm{j}k_{21,0n}l_2}\right|^2 + (a_{22}/a_1)^2\left|\sum_{n=0}^{p} G_{0n}^{+}\mathrm{e}^{-\mathrm{j}k_{22,0n}l_2}\right|^2\right\}. \quad (19)$$

Note that the non-planar modes leaving the chamber in outlet ducts will decay rapidly over a short distance due to smaller duct dimensions. The distance is chosen so that the effect of higher order modes on the transmission loss is negligible.

Setting $p = 0$ and $q = 0$ in equations (4), (6), (13), (15) and (17) readily gives the transmission loss for one-dimensional propagation inside an expansion chamber with double-outlet as

$$TL = 10\log_{10}\left[\frac{m_2}{4m_1}\left(1 + \frac{m_1}{m_2}\right)^2 + \frac{m_2}{4m_1}(m_1^2 - 1)\left(1 - \frac{1}{m_2^2}\right)\sin^2 kl\right], \quad (20)$$

where $m_1 = a^2/a_1^2$ and $m_2 = a^2/(a_{21}^2 + a_{22}^2)$. Within one-dimensional limitation, equation (20) is applicable for arbitrary number of outlets after accounting for the total area within the definition of m_2. For $m_1 = m_2 = m$, equation (20) reduces to the well-known limit of the simple expansion chamber:

$$TL = 10\log_{10}\left[1 + \frac{1}{4}\left(m - \frac{1}{m}\right)^2\sin^2 kl\right]. \quad (21)$$

3. RESULTS AND DISCUSSION

Two chambers are considered here with $l/d = 0{\cdot}205$ (short chamber) and $l/d = 1{\cdot}843$ (long chamber), and both with $d = 15{\cdot}32$ cm, $d_1 = d_{21} = d_{22} = 4{\cdot}86$ cm. The length and diameter of the expansion chamber were chosen to match two of the

nine configurations fabricated for the experiments of Selamet *et al.* [1,3]. Figures 2(a)–(d) compare the transmission loss of the short expansion chamber with double-outlet ($l/d = 0{\cdot}205$) from the present analytical approach and the boundary element method. The results are nearly identical throughout the frequency range of interest, supporting the validity of the present analytical approach. Also included in Figure 2 (as well as Figures 4 and 6) are the results from one-dimensional (axial) predictions in dotted lines for comparison purposes. The short chambers with double-outlet of Figures 2(a)–(d) clearly show no similarity between the one-dimensional (axial) and three-dimensional predictions due to dominant

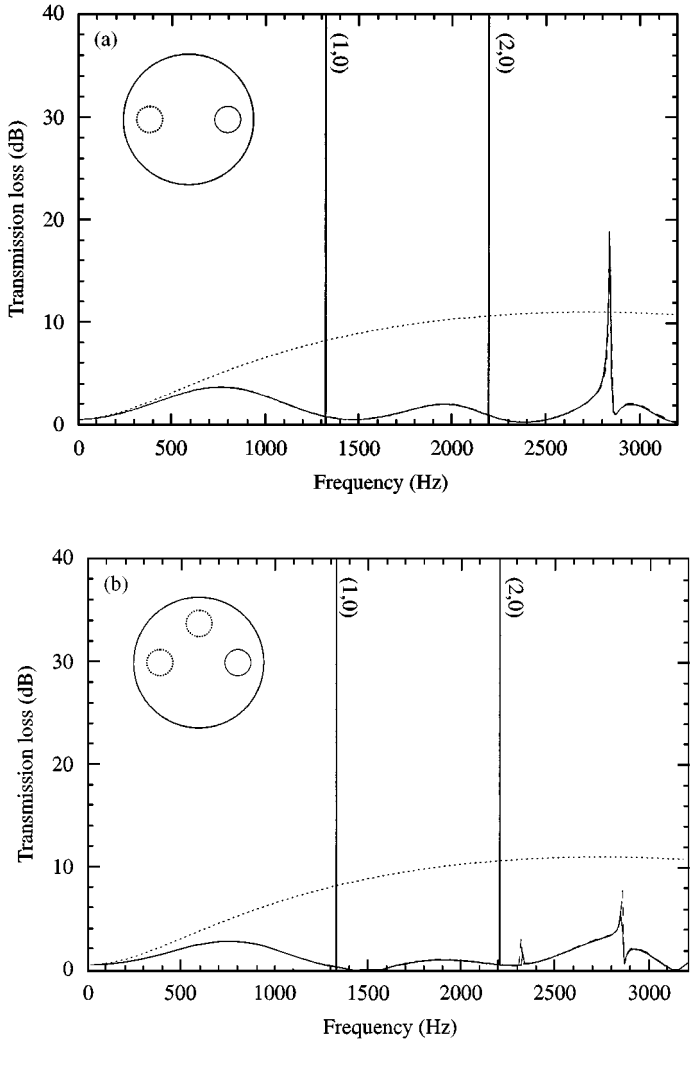

Figure 2. Transmission loss of short expansion chamber with offset inlet ($l/d = 0{\cdot}205$, $\delta_1 = 5{\cdot}10$ cm, $\delta_{22} = 5{\cdot}10$ cm): ——, 3-D analytical; – – –, BEM; ····· 1-D analytical. (a) $\delta_{21} = 5{\cdot}10$ cm, $\theta_{21} = 0^\circ$, $\theta_{22} = 180^\circ$; (b) $\delta_{21} = 5{\cdot}10$ cm, $\theta_{21} = 90^\circ$, $\theta_{22} = 180^\circ$; (c) $\delta_{21} = 5{\cdot}10$ cm, $\theta_{21} = 90^\circ$, $\theta_{22} = 270^\circ$; (d) $\delta_{21} = 0$ cm, $\theta_{21} = 0^\circ$, $\theta_{22} = 90^\circ$.

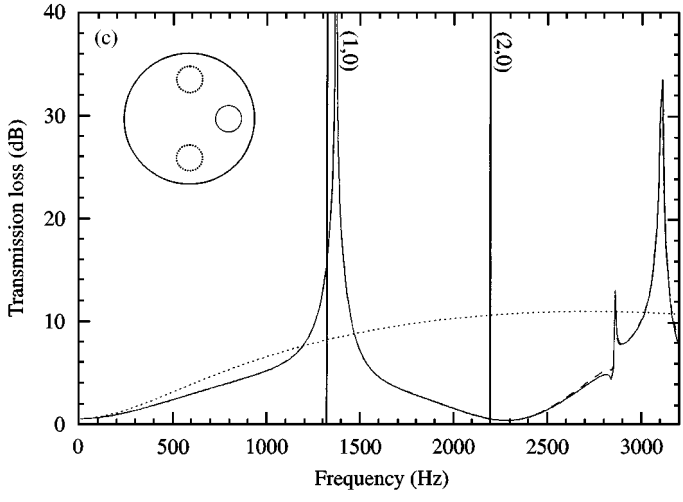

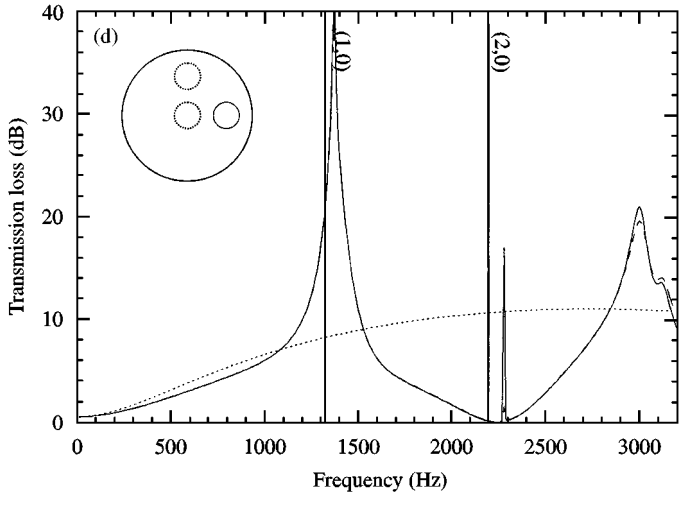

Figure 2. Continued.

transverse propagation. Figures 2(a) and (b) resemble the dome-like behavior due to one-dimensional propagation in the transverse direction within the chamber with a smaller effective expansion ratio, while Figures 2(c) and (d) show the dominant resonant peak, typical of a side-branch resonator. These characteristics are similar to that of the short expansion chambers with single-outlet. Figure 3 compares the analytical transmission loss results for the chambers with double-outlet (the configurations of Figure 2(b) and (c)) and those with single-outlet (180 and 90° offset). Both configurations have the same dimensions (length and diameter of chamber, diameters of inlet and outlet ducts). Except for the smaller acoustic attenuation due to smaller contraction ratio, the chamber with double-outlet of $\theta_{21} = 90^\circ$ and $\theta_{22} = 180^\circ$ shows the dome-like behavior similar to the chamber with 180° offset single-outlet, while the chamber with double-outlet of

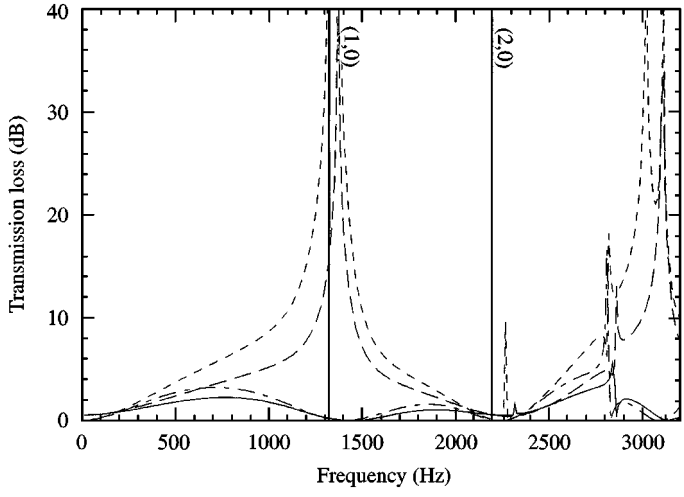

Figure 3. Transmission loss of short expansion chambers ($l/d = 0{\cdot}205$) with offset inlet: ——, double-outlet ($\theta_{21} = 90^\circ$, $\theta_{22} = 180^\circ$; from Figure 2(b)); – · – · –, single-outlet (180° offset); — —, double-outlet ($\theta_{21} = 90^\circ$, $\theta_{22} = 270^\circ$; from Figure 2(c)); – – –, single-outlet (90° offset).

$\theta_{21} = 90^\circ$ and $\theta_{22} = 270^\circ$ reveals the dominant resonant peak behavior similar to the chamber with 90° (or, equivalently 270°) offset single-outlet.

The transmission loss of the long expansion chamber with double-outlet ($l/d = 1{\cdot}843$) depicted in Figures 4(a)–(d) illustrate a good agreement between the analytical approach and the boundary element predictions. Figures 4(a)–(d) show the repeating one-dimensional attenuation dome behavior below the cut-off frequency of the first asymmetric (1, 0) mode. The acoustic attenuation in Figure 4(a) is reduced drastically as the multi-dimensional propagation begins to dominate above the cut-off frequency of the (1, 0) mode. This is due to the fact that the offset outlet arrangement with $\theta_{21} = 0^\circ$ and $\theta_{22} = 180^\circ$ can not eliminate the detrimental effect of (1, 0) mode. The attenuation in Figure 4(b) is similar to Figure 4(a), because the 180° offset outlet cannot eliminate the effect of the (1, 0) mode, although the 90° offset outlet has some impact on it. The effect of the asymmetric mode (1, 0) observed in Figures 4(a) and (b) could partially be eliminated by setting $\theta_{21} = 90^\circ$ and $\theta_{22} = 270^\circ$. As illustrated in Figure 4(c), the transmission loss increases over the cases of Figures 4(a) and (b), particularly in the frequency band between the (1, 0) and (2, 0) modes. While the concentric outlet is expected to improve the effect of all asymmetric modes, the attenuation behavior in Figure 4(d) remains, in general, similar to that in Figure 4(c). Figure 5 compares the analytical transmission loss results for the long chambers with double-outlet (the configurations of Figures 4(b) and (c)) and those with single-outlet (180 and 90° offset). Below the (1, 0) mode, the chambers with double-outlet exhibit the same number of domes as those with single-outlet. The attenuation with double-outlet is reduced somewhat due to a smaller contraction ratio. Above this mode, the chamber with double-outlet of $\theta_{21} = 90^\circ$ and $\theta_{22} = 180^\circ$ shows a low attenuation similar to the chamber with 180° offset single-outlet, while the chamber with double-outlet of $\theta_{21} = 90^\circ$ and

$\theta_{22} = 270^\circ$ reveals an improved attenuation similar to the chamber with 90° offset single-outlet.

In order to investigate the acoustic attenuation performance of expansion chamber with concentric inlet, the present three-dimensional analytical approach is applied to one specific configuration ($l = 12$ in, $d = 6$ in, $d_1 = d_{21} = d_{22} = 1$ in, $\theta_{21} = 0^\circ$, and $\theta_{22} = 180^\circ$) where the length and diameters match the configuration of the simple chamber with concentric inlet in reference [3]. Figure 6(a) ($\theta_{21} = 0^\circ$, $\theta_{22} = 180^\circ$, $\delta_{21} = \delta_{22} = 2{\cdot}60$ cm) shows the repeating dome behavior below the cut-off frequency of the first radial (0, 1) mode and the drastic reduction above this

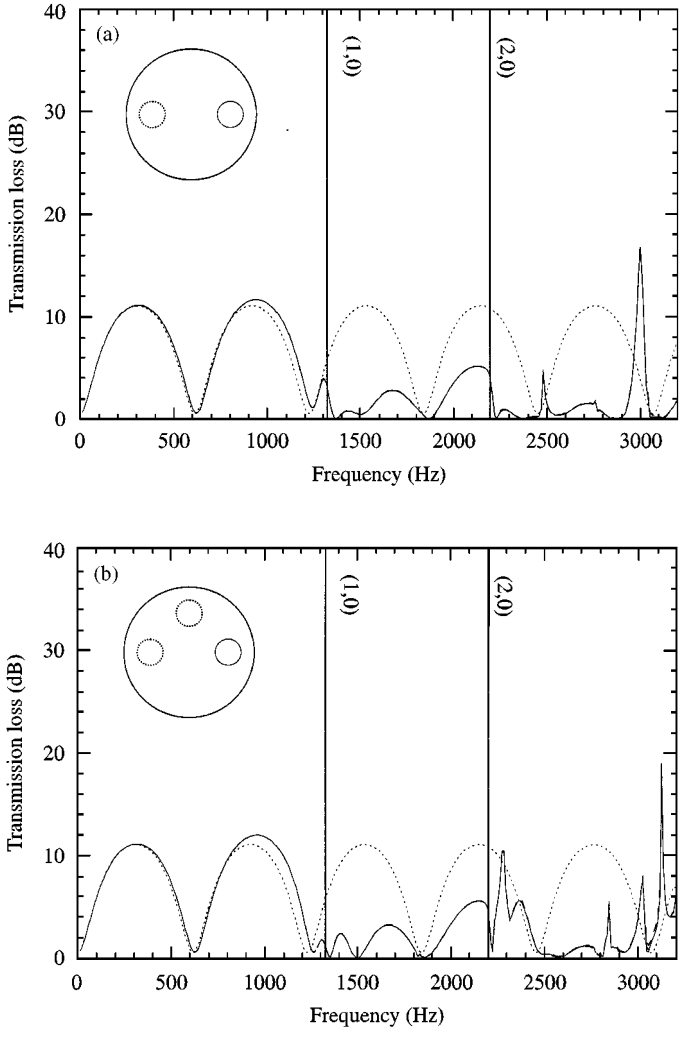

Figure 4. Transmission loss of long expansion chamber with offset inlet ($l/d = 1{\cdot}843$, $\delta_1 = 5{\cdot}10$ cm, $\delta_{22} = 5{\cdot}10$ cm): ——, 3-D analytical; – – –, BEM; ····· 1-D analytical. (a) $\delta_{21} = 5{\cdot}10$ cm, $\theta_{21} = 0^\circ$, $\theta_{22} = 180^\circ$; (b) $\delta_{21} = 5{\cdot}10$ cm, $\theta_{21} = 90^\circ$, $\theta_{22} = 180^\circ$; (c) $\delta_{21} = 5{\cdot}10$ cm, $\theta_{21} = 90^\circ$, $\theta_{22} = 270^\circ$; (d) $\delta_{21} = 0$ cm, $\theta_{21} = 0^\circ$, $\theta_{22} = 90^\circ$.

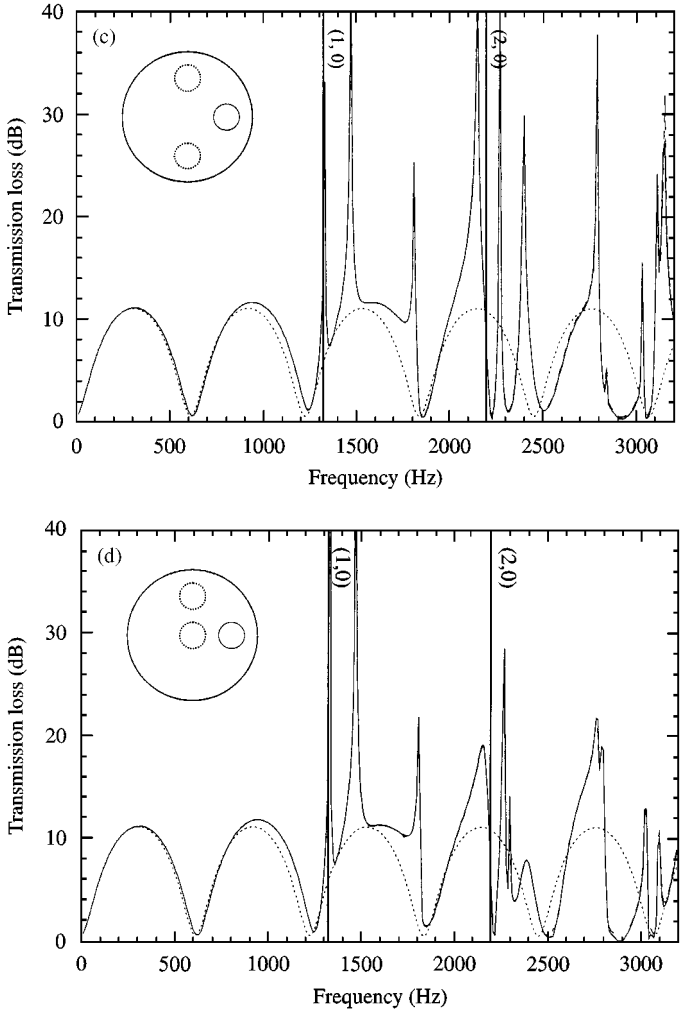

Figure 4. Continued.

mode, while Figure 6(b) ($\theta_{21} = 0^\circ$, $\theta_{22} = 180^\circ$, $\delta_{21} = \delta_{22} = 0{\cdot}6272a = 4{\cdot}78$ cm) extends the effective attenuation bands to the cut-off frequency of the (0, 2) mode. The improvement in Figure 6(b) is due to the fact that the two outlets are located on the pressure nodal circle of the (0, 1) mode, which eliminates the effect of this mode to a large extent. Figure 7 compares the analytical transmission loss results for the chamber with double-outlet (the configuration of Figure 6(b)) and the chamber with single-outlet ($\delta_{outlet} = 4{\cdot}78$ cm). The observations in this figure for concentric inlets are similar to those with offset inlets discussed earlier.

As with the simple expansion chambers, the relationship between the l/d ratio of the chamber and the number of repeating attenuation domes, kl/π, before higher order modes begin to dominate, may be expressed as

$$\frac{kl}{\pi} < \frac{2\alpha_{mn}}{\pi}\left(\frac{l}{d}\right). \tag{22}$$

For the expansion chambers with offset inlet, the number of domes can be approximated by substituting $\alpha_{10} = 1{\cdot}841$ into equation (22). By setting 90° relative offsets between inlet and outlets (or concentric and 90° offset outlets), the effect of the (1, 0) mode can partially be eliminated and the effective attenuation band is extended approximately to the (2, 0) mode; therefore, the number of domes (by

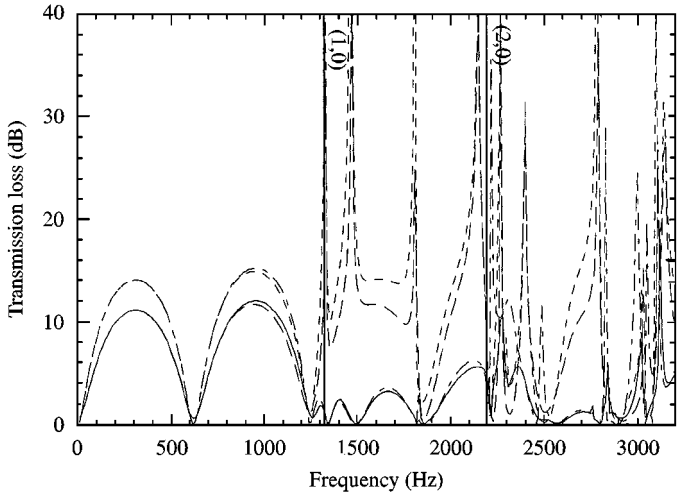

Figure 5. Transmission loss of long expansion chambers ($l/d = 1{\cdot}843$) with offset inlet: ——, double-outlet ($\theta_{21} = 90°$, $\theta_{22} = 180°$; from Figure 4(b)); – · – · –, single-outlet (180° offset); — —, double-outlet ($\theta_{21} = 90°$, $\theta_{22} = 270°$; from Figure 4(c)); – – –, single-outlet (90° offset).

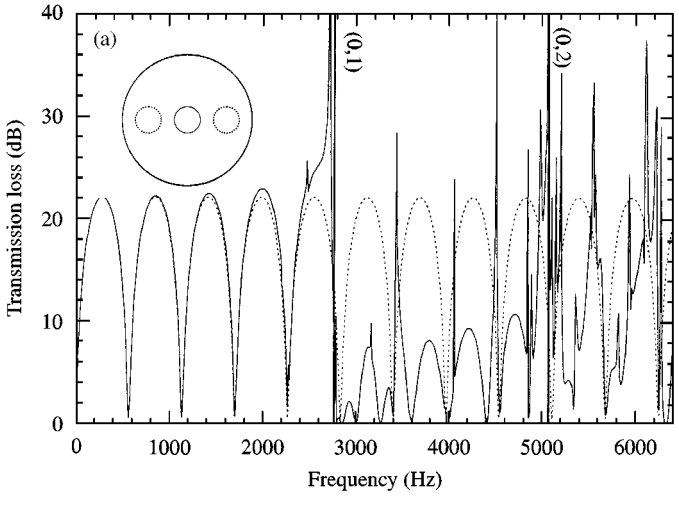

Figure 6. Transmission loss of expansion chamber with concentric inlet ($l/d = 2{\cdot}0$, $\delta_1 = 0$ cm, $\theta_{21} = 0°$, $\theta_{22} = 180°$): ——, 3-D analytical; ....., 1-D analytical. (a) $\delta_{21} = \delta_{22} = 2{\cdot}60$ cm; (b) $\delta_{21} = \delta_{22} = 4{\cdot}78$ cm.

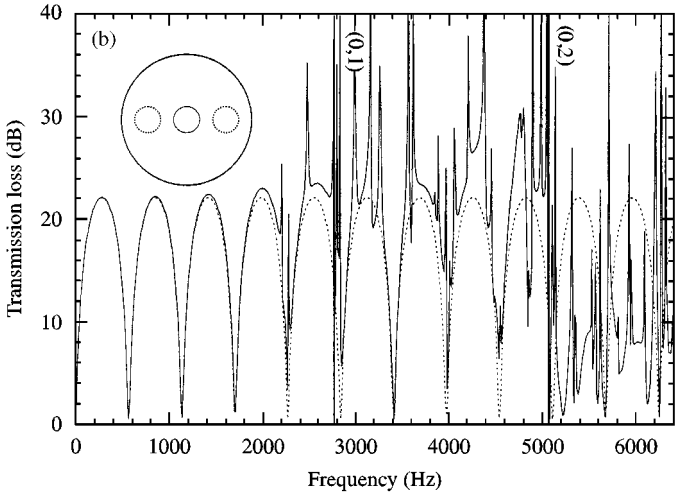

Figure 6. Continued.

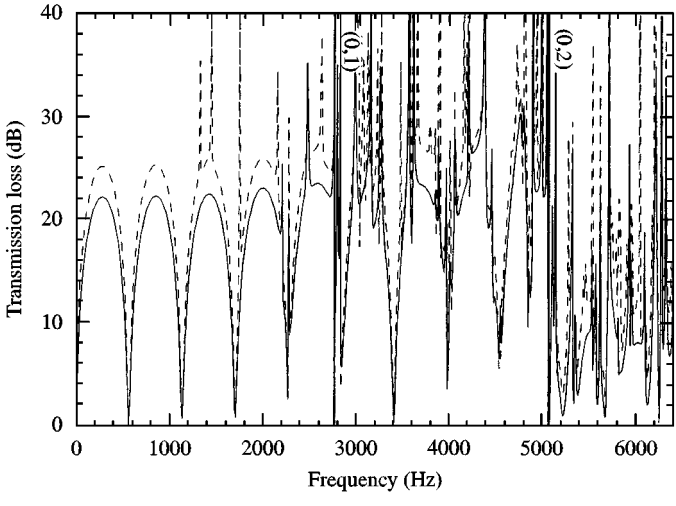

Figure 7. Transmission loss of expansion chambers with concentric inlet ($l/d = 2{\cdot}0$): ——, double-outlet (from Figure 6(b)); – – –, single-outlet ($\delta_{outlet} = 4{\cdot}78$ cm).

ignoring the numerous peaks) can be estimated by substituting $\alpha_{20} = 3{\cdot}054$ into equation (22). For the chambers with concentric inlet, the number of domes can be estimated by substituting $\alpha_{01} = 3{\cdot}832$ into equation (22). Offsetting two outlets by a radial distance of 0·6276 times the radius of the chamber eliminates the effect of the (0, 1) mode significantly. The effective attenuation band is then extended to the (0, 2) mode, approximately, thus the number of domes (by ignoring the numerous peaks) can be found by using $\alpha_{02} = 7{\cdot}016$ in equation (22). The number of 1-D (axial) attenuation domes in Figures 2, 4 and 6 is consistent with equation (22).

4. CONCLUDING REMARKS

A three-dimensional analytical approach is presented for the prediction of acoustic attenuation performance of circular expansion chambers with single-inlet and double-outlet, and compared with the boundary element predictions. The short chambers exhibit the dominant transverse propagation, while the long chambers show the repeating dome behavior. The number of domes (by ignoring the numerous peaks) can be approximated by introducing the value of corresponding α_{mn} into equation (22). For the same dimensions (length and diameter of chamber, diameters of inlet and outlet ducts), the double-outlet expansion chambers with offset inlet are shown to yield an acoustic behavior similar to offset single-outlet chambers: 90° configuration if the effect of the (1, 0) mode can be eliminated, 180° configuration otherwise. The double-outlet expansion chambers with concentric inlet also exhibit an attenuation similar to single-outlet chambers with concentric inlet. The slight reduction in acoustic performance of double-outlet mufflers is expected, in general, to be more than offset by their potential advantage in terms of reduction of flow noise and backpressure.

REFERENCES

1. A. Selamet and P. M. Radavich 1977 *Journal of Sound and Vibration* **201**, 407–426. The effect of length on the acoustic attenuation performance of concentric expansion chambers: an analytical, computational, and experimental investigation.
2. A. Selamet and Z. L. Ji 1998 *Journal of Sound and Vibration* **213**, 601–617. Acoustic attenuation performance of circular expansion chambers with offset inlet/outlet: I. Analytical approach.
3. A. Selamet, Z. L. Ji and P. M. Radavich 1998 *Journal of Sound and Vibration* **213**, 619–641. Acoustic attenuation performance of circular expansion chambers with offset inlet/outlet: II. Analytical, computational and experimental study.
4. L. J. Erikkson 1980 *Journal of the Acoustical Society of America* **68**, 545–550. Higher order mode effects in the circular ducts and expansion chambers.
5. L. J. Eriksson 1982 *Journal of the Acoustical Society of America* **72**, 1208–1211. Effect of inlet/outlet locations on higher order modes in silencers.
6. A. Craggs 1976 *Journal of Sound and Vibration* **48**, 377–392. A finite element method for damped acoustic systems: an application to evaluate the performance of reactive mufflers.
7. A. D. Sahasrabudhe, S. A. Ramu and M. L. Munjal 1991 *Journal of Sound and Vibration* **147**, 371–394. Matrix condensation and transfer matrix techniques in the 3-D analysis of expansion chamber mufflers.
8. A. F. Seybert and C. Y. R. Cheng 1987 *Journal of Vibration, Acoustics, Stress, and Reliability in Design* **109**, 15–21. Application of the boundary element method to acoustic cavity response and muffler analysis.
9. C. Y. R. Cheng and A. F. Seybert 1991 *Journal of Sound and Vibration* **151**, 119–129. A multidomain boundary element solution for silencer and muffler performance prediction.
10. Z. L. Ji, Q. Ma and Z. H. Zhang 1994 *Journal of Sound and Vibration* **173**, 57–71. Application of the boundary element method to predicting acoustic performance of expansion chamber mufflers with mean flow.
11. P. A. Nelson and C. L. Morfey 1981 *Journal of Sound and Vibration* **79**, 263–289. Aerodynamic sound production in low speed flow ducts.

12. A. J. GREEN and P. N. SMITH 1988 *IMechE Conference Proceedings*, *MEP*-297, C77/88, 45–54. Gas flow noise and pressure loss in heavy vehicle exhaust systems.
13. J. KUNZ and P. GARCIA 1995 *SAE Technical Paper* 950546. Simulation and measurement of hot exhaust gas flow with a cold air flow bench.
14. M. L. MUNJAL 1987. *Acoustics of Ducts and Mufflers*. New York: Wiley–Interscience.

APPENDIX A: SOUND PROPAGATION IN CIRCULAR DUCT

The three-dimensional sound propagation in a duct with no bulk flow is governed by the well-known Helmholtz equation [14]

$$\nabla^2 P + k^2 P = 0, \tag{A1}$$

where P is the acoustic pressure, k is the wavenumber. The acoustic pressure can be expressed, for a wave C travelling in the positive z-direction in a circular rigid duct of radius a, as

$$P_C = \sum_{m=0}^{\infty}\sum_{n=0}^{\infty} C_{mn}^{+} J_m(\alpha_{mn} r/a) \mathrm{e}^{\mathrm{j}m\theta} \mathrm{e}^{-\mathrm{j}k_{mn}z} + \sum_{m=1}^{\infty}\sum_{n=0}^{\infty} C_{mn}^{-} J_m(\alpha_{mn} r/a) \mathrm{e}^{\mathrm{j}m\theta} \mathrm{e}^{\mathrm{j}k_{mn}z}, \tag{A2}$$

and, for a wave D travelling in the negative z-direction, as

$$P_D = \sum_{m=0}^{\infty}\sum_{n=0}^{\infty} D_{mn}^{+} J_m(\alpha_{mn} r/a) \mathrm{e}^{-\mathrm{j}m\theta} \mathrm{e}^{-\mathrm{j}k_{mn}z} + \sum_{m=1}^{\infty}\sum_{n=0}^{\infty} D_{mn}^{-} J_m(\alpha_{mn} r/a) \mathrm{e}^{\mathrm{j}m\theta} \mathrm{e}^{-\mathrm{j}k_{mn}z}, \tag{A3}$$

where C_{mn}^{+}, C_{mn}^{-}, D_{mn}^{+} and D_{mn}^{-} are the complex coefficients with the superscripts $+$ and $-$ designating the positive and negative θ directions; (r, θ, z) is the cylindrical co-ordinates; $J_m(x)$ is the Bessel function of the first kind of order m; α_{mn} is the root satisfying the radial boundary condition of $J'_m(\alpha_{mn}) = 0$; m and n denote the asymmetrical and radial mode numbers; and

$$k_{mn} = k[1 - (\alpha_{mn}/ka)^2]^{1/2} \tag{A4}$$

is the axial wavenumber of the mode (m, n). For a rigid duct, a propagating wave has $k > \alpha_{mn}/a$ so that k_{mn} is real and $\mathrm{e}^{-\mathrm{j}k_{mn}z}$ does not decay in z; an evanescent wave has $k < \alpha_{mn}/a$ so that k_{mn} is negative imaginary and $\mathrm{e}^{-\mathrm{j}k_{mn}z}$ decays exponentially in z. The axial particle velocities for waves C and D are obtained from the linearized momentum equation, $\mathrm{j}\rho\omega U = -\partial P/\partial z$, as

$$U_C = \frac{1}{\rho\omega}\left\{ \sum_{m=0}^{\infty}\sum_{n=0}^{\infty} k_{mn} C_{mn}^{+} J_m(\alpha_{mn} r/a) \mathrm{e}^{-\mathrm{j}m\theta} \mathrm{e}^{-\mathrm{j}k_{mn}z} + \sum_{m=1}^{\infty}\sum_{n=0}^{\infty} k_{mn} C_{mn}^{-} J_m(\alpha_{mn} r/a) \mathrm{e}^{\mathrm{j}m\theta} \mathrm{e}^{-\mathrm{j}k_{mn}z} \right\}, \tag{A5}$$

and

$$U_D = -\frac{1}{\rho\omega}\left\{\sum_{m=0}^{\infty}\sum_{n=0}^{\infty} k_{mn} D_{mn}^{+} J_m(\alpha_{mn} r/a) \mathrm{e}^{-\mathrm{j}m\theta} \mathrm{e}^{\mathrm{j}k_{mn}z} + \sum_{m=1}^{\infty}\sum_{n=0}^{\infty} k_{mn} D_{mn}^{-} J_m(\alpha_{mn} r/a) \mathrm{e}^{\mathrm{j}m\theta} \mathrm{e}^{\mathrm{j}k_{mn}z}\right\}, \tag{A6}$$

where ρ is the medium density, and ω is the angular frequency.

APPENDIX B: NOMENCLATURE

a	radius of chamber
a_1	radius of inlet duct
a_{21}, a_{22}	radii of outlet ducts
A, B, C, D, E, F, G, H	pressure coefficients
j	$=\sqrt{-1}$, imaginary unit
$J_m(x)$	Bessel function of the first kind of order m
k_{mn}	axial wavenumber in chamber
$k_{1,mm}$	axial wavenumber in inlet duct
$k_{21,mn}, k_{22,mn}$	axial wavenumbers in outlet ducts
l	length of expansion chamber
m	asymmetric mode number
n	radial mode number
p	number of m-terms after truncation
P	acoustic pressure
q	number of n-terms after truncation
(r, θ, z_1)	cylindrical co-ordinate system for chamber
(r_1, φ, z_1)	cylindrical co-ordinate system for inlet duct
s	orthogonal expansion terms
S	cross-sectional area of chamber
S_1	cross-sectional area of inlet duct
S_{21}, S_{22}	cross-sectional areas of outlet ducts
t	orthogonal expansion terms
U	axial particle velocity
α_{mn}	zeros of $J'_m(\alpha_{mn}) = 0$
δ_1	inlet offset distance from the center of chamber
δ_{21}, δ_{22}	outlet offset distances from the center of chamber
θ_{21}, θ_{22}	relative angles between inlet and outlets